Effects of Additives on the Morphology of Solution Phase Aggregates formed by Active Layer Components of High-Efficiency Organic Solar Cells

Sylvia J. Lou[†‡], Jodi M. Szarko[†‡], Tao Xu[§], Luping Yu[‡§], Tobin J. Marks*[†‡], Lin X. Chen*[†‡ǁ]

[†] Department of Chemistry, Northwestern University, 2145 Sheridan Road, Evanston, Illinois 60208, United States

[‡] The Argonne-Northwestern Solar Energy Research (ANSER) Center, Northwestern University, Evanston, Illinois 60208, United States

[§] Department of Chemistry and James Franck Institute, The University of Chicago, 929 East 57th Street, Chicago, Illinois 60637, United States

[ǁ] Chemical Sciences and Engineering Division, Argonne National Laboratory, 9700 South Cass Avenue, Argonne, Illinois, 60439

Corresponding authors: l-chen@northwestern.edu; t-marks@northwestern.edu; lupingyu@chicago.edu

Solution Preparation

The synthesis of **PTB7** has been described previously.[1] The **PTB7** (10 mg/mL; M_n = 42 KD, PDI=2.2) and **PC$_{70}$BM** (15 mg/mL, Sigma Aldrich >99%) were dissolved in anhydrous chlorobenzene (CB; Sigma Aldrich) in a dry N_2 glove box (<1ppm O_2, <1 ppm H_2O). The solutions were heated and stirred overnight at 40°C to ensure complete dissolution of the **PTB7**. Next, 1,8-diiodooctane (DIO; Sigma Aldrich >98%; 3% v/v) was added to selected solutions 1 h prior to characterization. All samples were removed from heat 1 h prior to characterization.

Small-angle x-ray scattering experiments

Small-angle x-ray scattering (SAXS) measurements were performed using Beamline 5ID of the Advanced Photon Source (APS) at Argonne National Laboratory. Solution scattering was performed in the transmission mode using a collimated x-ray beam of 7 keV. To minimize x-ray damage, solutions were characterized in a 1.5 mm quartz flow cell with a flow rate of 10 μL/s. The flow cell was thoroughly cleaned between samples with CB. Data were collected using a two-dimensional area MAR detector which was situated 1500 mm from the sample. For each sample, a CB scattering exposure was taken immediately before the sample was exposed for use in solvent background subtraction.

X-ray scattering fitting procedures

Solvent subtraction For each sample scattering signal, the chlorobenzene (CB) scattering signal (Figure S1) was subtracted. Due to the strong scattering of the CB solvent, it is difficult to completely remove the solvent scattering at higher Q (Q>0.6 Å^{-1}). In both the samples and solvent traces, we see an intensity decrease as q increases. While this high
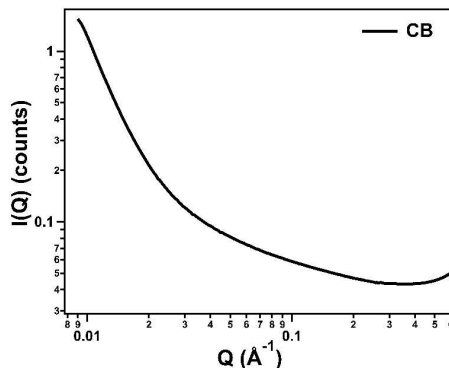
Figure S1. Scattering signal from CB solvent without DIO. There is no change in the scattering upon addition of 3% DIO.

scattering signal at low Q can indicate large aggregates, we believe that it can be attributed to experimental set-up used in which an exponential decrease of scattering intensity is frequently seen especially for this lower Q (Q < 0.5 Å^{-1} regime).

Standard Modeling I: Data were fit using the Standard Modeling I fit program developed by Jan Ilavsky.[2] The program is based on the standard small-angle scattering equation,

$$I(Q) = |\Delta\rho|^2 \int_0^\infty |F(Q,r)|^2 V(r)^2 NP(r) dr \qquad (1)$$

where *I(Q)* is intensity, $\Delta\rho$ is the difference in electron density between the scattering particle and the surrounding medium, *F(Q,r)* is the form factor, *V(r)* is the particle volume, *N* is the total number of particles that scatter, and *P(r)* is the probability of a scattering particle with radius *r*. Each x-ray scattering trace was fit assuming either two (**PC$_{71}$BM** with and without DIO) or three (all other traces) log normal distributions of aggregate sizes. This model is intended to find a mean radius and number distribution of spherical aggregates. We assume that all of the peaks present are due to an aggregation dimension rather than the form factor, a shape dependent function, of the aggregate. A step-by-step description of the regional fitting of **PTB7** without DIO is shown below based on three Q regions: Q>0.3 Å^{-1}, 0.1 Å^{-1}<Q<0.3 Å^{-1}, and Q<0.1 Å^{-1}.

Starting at the high Q regime we calculate the first size distribution (Figure S2) allowing the mean size, distribution width, and aggregate volume to vary.
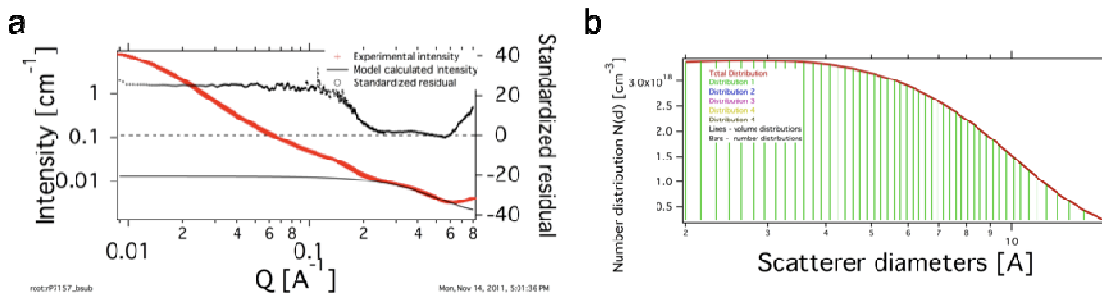

Figure S2. Level 1 distribution of peak in high Q regime (Q ~0.4 Å^{-1}): a) fit and residual, and b) log normal distribution.

S 2

We next fit the second highest peak which we will attribute to aggregate size again allowing mean size, aggregate volume, and distribution width to vary.
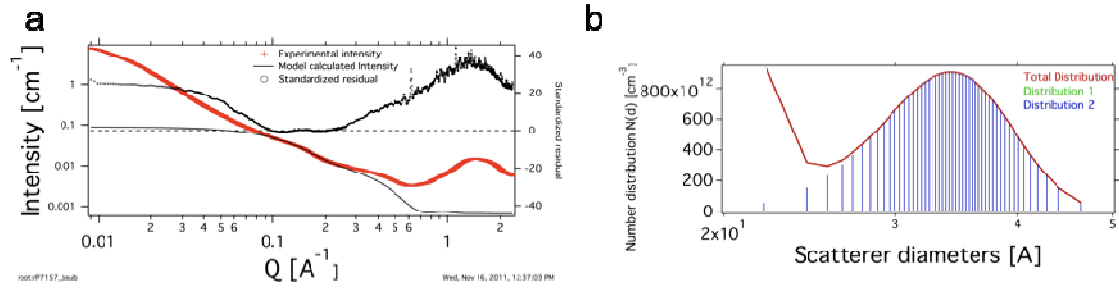

Figure S3. Level 2 distribution of peak in middle Q regime (Q ~0.15 Å^{-1}): a) fit and residual, and b) log normal distribution.

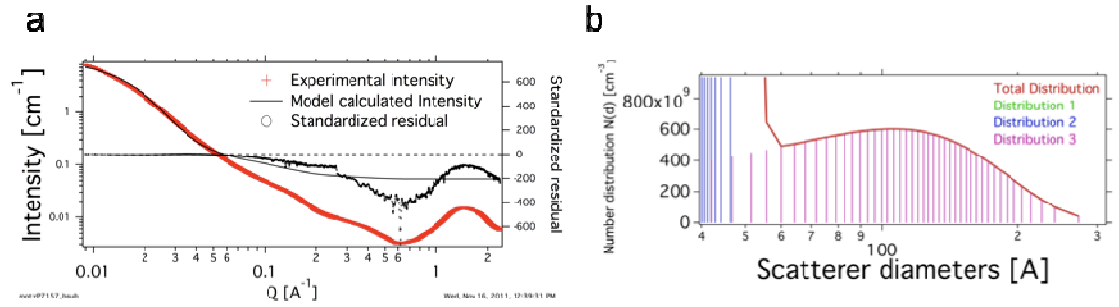We then fit the low q regime (0.01 Å^{-1} < q < 0.1 Å^{-1}).

Figure S4. Level 3 distribution of peak in the low Q regime (Q <0.1 Å^{-1}): a) fit and residual, and b) log normal distribution (pink).

Finally, holding the mean size constant, the entire scattering trace was fit using all three distributions (Figure **S5**).
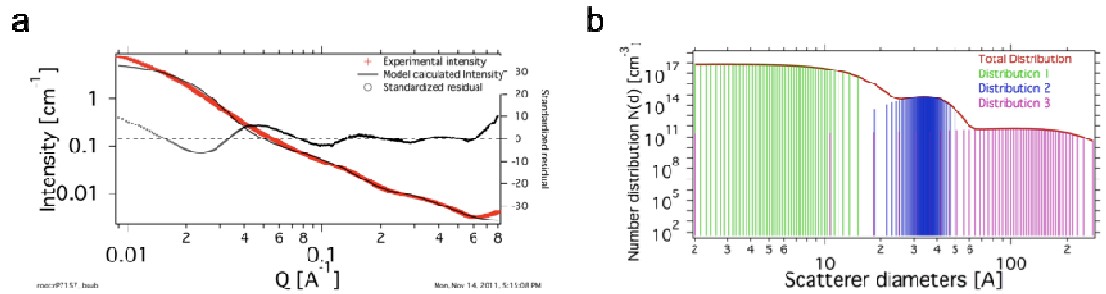

Figure S5. a) Total fit of **PTB7** curve using all three distributions. b) Total distribution of scatterer diameter sizes. Distributions are color coded so that distribution 1 (green) corresponds to the Level 1 fit (high Q), distribution 2 (blue) corresponds to the Level 2 fit (mid Q), and distribution 3 (pink) corresponds to the Level 3 fit (low Q). The total distribution is shown in red.

Modeling I, Standard Model fits for PTB7:PC₇₁BM samples

Here we show the similarity between the scattering signals of **PTB7:PC$_{71}$BM** blend with and without DIO and fit them using Modeling I (Figure S3). The similarity between the traces indicates that scattering from **PTB7** domains dominates the blend profile and therefore, a component analysis in which the relative contributions of the active layer components is analyzed was performed (Figure 2c, d).
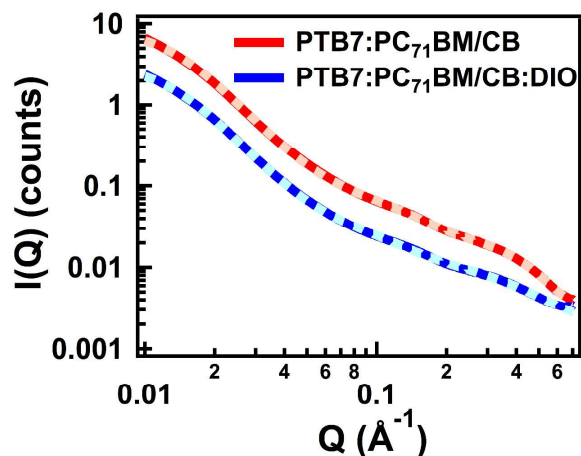

Figure S6. Standard Modeling I fit for **PTB7:PC$_{71}$BM** blend solutions assuming three Gaussian distributions of aggregates. **PTB7**:**PC$_{71}$BM**/CB:DIO is offset by half.

We also confirm that there is a small change in the **PC$_{71}$BM** aggregate size upon addition of **PTB7** in the blend solution, but the trend of decreasing aggregate size is still evident. To obtain these traces, the **PTB7** component from the component fits (Figures 2c, d) was subtracted from the blend traces leaving only the **PC$_{71}$BM** component.
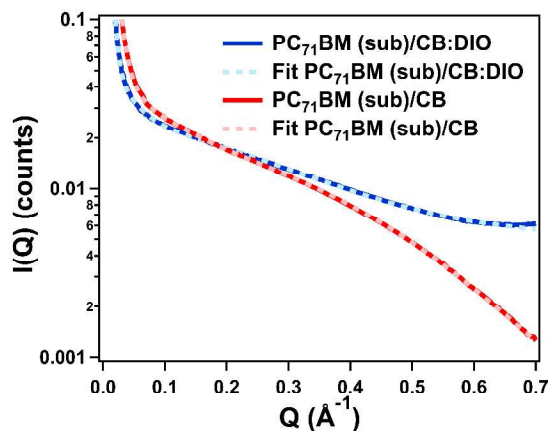

Figure S7. Fits of **PC$_{71}$BM** traces obtained by subtracting **PTB7** component fit from the blend traces.

Unified fit: The data was confirmed with a second fitting method, the Unified Fit which includes contributions from the two main regimes in small angle scattering – the Guinier region and the Porod region.[3] The Guinier and Porod equations are based on approximations in the small angle scattering equation in the high and low q regimes. The Guinier equation

$$I(Q) = \rho_0^2 v^2 e^{-\frac{q^2 R_g^2}{3}}$$
(2)

where *I(Q)* is scattering intensity, ρ_0 is the average scattering length density, *v* is volume, and R_g is the radius of gyration, dominates the scattering intensity in the low *Q* regime. The Porod equation

$$I(Q) = \frac{2\pi(\Delta\rho)^2 S}{Q^4}$$
(3)

where $\Delta\rho$ is the difference in electron density between the solute and solvent and *S* is the boundary surface area between the aggregate and solvent. The Porod equation is used in the high *Q* regime. The terms low *Q* and high *Q* are generally system dependent, but the Guinier is valid for $QR_g < 1$ and Porod is valid for $QR_g > 1$. Both of these approximations can be used to determine the size and shape of the aggregate, and texture of the aggregate surface in dilute solutions.

Unified fits are shown in Figure S6 and the mean radii are given in Table S1.

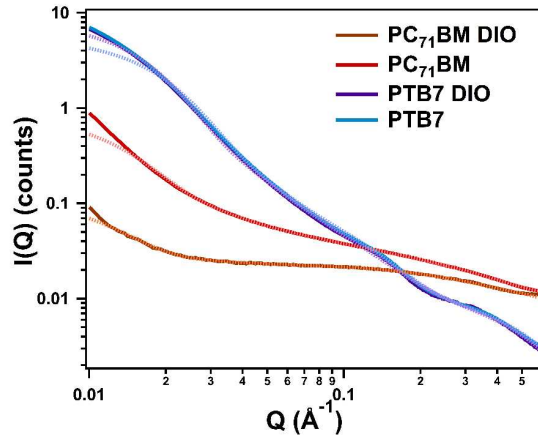The mean radii of PCBM are similar to what we find using Modeling I. The difference in

Figure S6. Unified fits for **PTB7** and **PC$_{71}$BM** scattering traces with and without DIO. Solid lines are experimental data and overlaid dotted lines are fits.

PTB7 values may be due to a less uniform aggregation in **PTB7**, meaning a wider distribution of shapes and rougher surfaces. This would increase the impact of Porod fit of **PTB7** in the high Q regime. For all the fits, the power law is around 2 far from the ideal Porod value of 4 indicating that all of the aggregates are fairly rough. Because Modeling I predicts similar aggregation sizes for the **PC$_{71}$BM** and trends for both systems as the Unified fit, we chose to use Modeling I fits for this size analysis.

Table S1: Comparison of mean radius using Standard Modeling I and the Unified Fit.

Mean radius (Å)	Standard Modeling I	Unified Fit
PTB7	183 ± 10	113 ± 6
	34.2 ± 0.4	19.6 ± 1.8
	<7 (fit to 3.0 ± 0.6)	5.4 ± 1.5
PTB7 with DIO	174 ± 12	140 ± 2
	36.7 ± 0.8	18.3 ± 5.2
	<7 (fit to 4.1 ± 0.3)	5.7 ± 1.2
PC71BM	235 ± 23	170 ± 3
	11.5 ± 0.5	12.6 ± 0.3
PC71BM with DIO	240 ± 35	197 ± 2
	5.7 ± 1.1	5.2 ± 2.1
PC71BM from PTB7:PC71BM blend	9.8 ± 0.2	13.2 ± 0.8
PC71BM from PTB7:PC71BM with DIO	<7 (fit to 4.1 ± 0.3)	<7 (fit to 4.4 ± 0.2)

While only the smaller domains were discussed here in detail, these are hierarchical structures, so the size of the smaller aggregates are related to the size of larger aggregates and both will impact the resulting film. Because we were interested in understanding the solubility of **PTB7** and **PC$_{71}$BM**, we chose to study the smaller aggregates in order to clearly see the decrease in aggregate size. Based on our knowledge of the resulting film morphology from TEM images[1] we know that the domain size in film is about 10 nm for films spin coated from the CB:DIO solution and we selected the Q range to include 10 nm aggregates. While it is possible that larger aggregates do impact the resulting film, we believe that it is more likely that smaller aggregates in solution will join together to make larger aggregates in the film rather than larger aggregates breaking apart to form the 10 nm domains.

References

(1) Liang, Y. Y.; Wu, Y.; Feng, D. Q.; Tsai, S. T.; Son, H. J.; Li, G.; Yu, L. P. *J Am. Chem. Soc.* **2009,** *131* (1), 56-57.

(2) Ilavsky, J., Modelling I, Standard Models. *Igor Pro 6.2* **2007**.

(3)   Beaucage, G. *J Appl. Cryst.* **1995**, *28*, 717-728.; Beaucage, G. *J Appl. Cryst.* **1996**, *29*, 134-146.; Beaucage, G.; Rane, S.; Sukumaran, S.; Satkowski, M.M.; Schechtman, L.A.; Doi, Y. *Macromol.* **1997**, *30*, 4158-4162.